Electrochimica Acta 55 (2010) 1687–1695

Contents lists available at ScienceDirect

Electrochimica Acta

journal homepage: www.elsevier.com/locate/electacta

Chemical deposition of platinum on metallic sheets as counterelectrodes for dye-sensitized solar cells

Chih-Ming Chen [a,*], Chia-Hsien Chen [a], Tzu-Chien Wei [b]

[a] Department of Chemical Engineering, National Chung Hsing University, 250 Kuo-Kuang Rd., Taichung 402, Taiwan
[b] Hsin-Chu Laboratory, Tripod Technology Corporation, No. 106, Dongmei Rd., East District, Hsinchu 300, Taiwan

ARTICLE INFO

Article history:
Received 6 July 2009
Received in revised form 17 October 2009
Accepted 20 October 2009
Available online 29 October 2009

Keywords:
Platinum
Chemical deposition
Stainless steel
Nickel
Counterelectrode

ABSTRACT

Platinum (Pt) layers were grown on metallic sheets, either stainless steel or nickel (Ni), by chemical deposition, and the resulting Pt-coated metallic sheets were used as counterelectrodes for dye-sensitized solar cells (DSSCs). Compared with other methods of depositing Pt layers, chemical deposition is simple, low-temperature, and easy to scale-up for industrial applications. Thin metallic sheets were employed as the substrates for the Pt deposition because of their low cost, excellent electrical conduction capability, and flexibility. The Pt concentration of the plating solution plays an important role in the photovoltaic performance of the DSSC; higher Pt concentrations correlate with better photovoltaic performance. The DSSCs that use Ni sheets coated with chemically deposited Pt as the counterelectrodes were found to have lower series and charge transfer resistances compared with those based on stainless steel. The Ni-based DSSCs also exhibit higher fill factors and short-circuit currents, and therefore, better energy conversion efficiency. The best efficiency observed with the Ni-based DSSCs was 7.29%.

1. Introduction

Dye-sensitized solar cells (DSSCs) have received much attention recently because they are promising photovoltaic devices that can generate energy. In addition, these types of cells have many advantages, such as low material cost, easy fabrication, and high efficiency for energy conversion [1–3]. A typical DSSC consists of three main components: a photoanode, a counterelectrode, and an electrolyte. The photoanode is constructed of a dye-adsorbed nanocrystalline TiO_2 film deposited on a transparent conducting oxide (TCO) glass substrate, such as indium-doped tin oxide (ITO) or fluorine-doped tin oxide (FTO). A second TCO glass substrate is used as the counterelectrode. An iodide–triiodide redox couple in an organic solvent is used as the electrolyte that transports charged ions between these two electrodes. A catalytic material is usually coated on the counterelectrode to assist in the reduction of triiodide (I_3^-) ions. Although many other catalytic materials have been proposed for use in DSSCs (e.g., carbon [4–8] and conductive polymers [9–11]), platinum (Pt) is still considered to have superior electrocatalytic activity for triiodide reduction because the DSSCs that use Pt-coated counterelectrodes exhibit better efficiency [12–20].

Sputtering is commonly used to deposit a thin Pt layer onto the TCO glass substrate [12,13]. However, this process requires an ultrahigh vacuum, which is not cost efficient. Thermal deposition [14–16] is also frequently employed to grow a thin Pt layer; in this procedure, a drop of precursor solution (hexachloroplatinic acid, H_2PtCl_6) is spread onto a TCO glass substrate, followed by annealing at 380 °C. This approach can produce a Pt layer with low Pt loading and excellent catalytic performance, but the high-temperature annealing process precludes the use of thermal deposition with temperature-sensitive substrates like plastic boards. Electrochemical reduction has also been used to grow the Pt layer [17–20], and this process is a simple, low-temperature, and economical method that requires neither ultrahigh vacuum nor high-temperature annealing treatment. Yoon et al. [20] prepared a counterelectrode by electrodeposition of a mesoporous Pt layer onto a FTO glass substrate. The DSSC based on this electrodeposited-Pt counterelectrode shows higher energy conversion efficiency compared to other cells with Pt electrodes that were fabricated via sputtering or thermal deposition.

Chemical deposition is another electrochemical approach for growing a thin metallic layer. Compared to electrodeposition, chemical deposition can be carried out without an applied potential, and it does not require vacuum environment or high-temperature annealing. In addition, this process requires low energy inputs and can easily be scaled-up for industrial applications. However, chemical deposition is rarely employed for growing Pt layers on counterelectrodes for DSSCs.

Thin metallic sheets have also been employed as the counterelectrode substrates for DSSCs. Compared with the commonly used TCO glass substrates, metallic substrates are superior in terms of both the material cost and the electrical conduction capability

* Corresponding author. Tel.: +886 4 22859458; fax: +886 4 22854734.
E-mail address: chencm@nchu.edu.tw (C.-M. Chen).

0013-4686/$ – see front matter © 2009 Elsevier Ltd. All rights reserved.
doi:10.1016/j.electacta.2009.10.050

[21,22]. In addition, thin metallic sheets are flexible, which enables the preparation of flexible DSSCs. One drawback of using metallic substrates in DSSCs is that the liquid electrolytes may corrode the metals. Ma et al. [22] investigated several types of metallic substrates and found that stainless steel (SUS304) and nickel have good stability in liquid electrolytes containing I^-/I_3^- redox species. They also found that using stainless steel as the counterelectrode for large-scale DSSCs produced higher fill factors and energy conversion efficiencies than DSSCs using glass substrates, and this result is due to the lower sheet resistance of metals. Various deposition methods, such as sputtering, electroplating, and thermal deposition, were employed for growing Pt layers on stainless steel sheets. However, chemical deposition has not yet been used with metallic substrates.

In the present study, the counterelectrode was prepared by chemical deposition of Pt on metallic substrates. Following the precedent of Ma et al. [22], the metallic substrates were either stainless steel (SUS 304) or nickel. The morphologies of the deposited Pt layers on the two types of metallic sheets were studied and characterized. The electrochemical impedance of these counterelectrodes was measured, and the photovoltaic performance of the corresponding DSSCs was also examined.

2. Experimental procedures

2.1. Preparation of counterelectrodes

The plating solution was prepared by dissolving 1 g of H_2PtCl_6 in 100 mL of 4% HCl, followed by taking 0.01, 0.02, 0.05, 0.1, 0.2, 0.5, and 1 mL of H_2PtCl_6 solution and diluting each to 12.5 mL with deionized water. The Pt concentrations in the solutions were 3.12, 6.24, 15.6, 31.2, 62.4, 156, and 312 mg/L, respectively. Two types of metallic sheets (2 cm × 2 cm in size), stainless steel (SUS 304, Alfa Co., 100 μm thick) and nickel (Alfa Co., 50 μm thick), were used for the chemical deposition of Pt. The metallic sheets were polished with fine sandpaper and with Al_2O_3 suspensions, and then they were cleaned ultrasonically in acetone to remove oxides and other surface contaminants. Next, the metallic sheets were immersed in the plating solution at 67–70 °C. Typically, the temperature has a significant effect on the deposition rate. At lower temperatures, the deposition nearly stops, but at higher temperatures, some components of the plating solution may evaporate more quickly than desired. Therefore, moderate temperatures (67–70 °C) were employed.

When the metallic sheets were immersed in the plating solution, the color of the solution changed gradually from yellow to colorless, indicating that the $[PtCl_6]^{2-}$ ions were reduced and that, simultaneously, the resultant Pt atoms were deposited on the metallic substrates. The chemical deposition method used in the present work involves two steps. First, platinum is deposited on the metallic substrates by displacement, and second, electroless deposition takes place. Platinum can be deposited on some metallic substrates (e.g., nickel and stainless steel) by displacement in a solution of H_2PtCl_6. However, only the very top layer of the metallic substrate is replaced with Pt. In order to study the effects of various Pt loadings on the cell performances, the Pt layer was thickened by repeating the deposition process, using the first Pt layer as the catalyst for subsequent depositions. The latter process is known as electroless deposition. In the electroless deposition process, hydrazine (3.2 g/L) was used as the reductant.

The chemical deposition was complete when the solution became completely colorless (i.e., when $[PtCl_6]^{2-}$ was completely reduced), which required approximately 5–20 min, depending upon the concentration of the plating solution. To further validate the reduction conditions, the adsorption curves of the solutions before and after reduction were measured using a UV–vis spectrophotometer (UV-1601, Shimadzu, Japan).

For comparison, Pt layers were sputtered onto the metallic sheets for use as the counterelectrodes for DSSCs. The sputtered Pt layers on the stainless steel and nickel are 100-nm thick, with Pt loading levels of 200 μg/cm^2 [23].

2.2. Characterization of surface morphologies of chemically deposited and sputtered Pt layers on metallic substrates

The surface microstructures of chemically deposited and sputtered Pt layers on metallic substrates were observed using a scanning electron microscope (SEM). The deposited Pt layers were also examined using an atomic force microscope (AFM), and the values of root-mean-square roughness (R_{rms}) of the Pt layers were obtained from the AFM data.

2.3. Analysis of the electrochemical impedance spectroscopy (EIS)

EIS analysis was used to measure the catalytic activities of chemically deposited and sputtered Pt in the reduction of triiodide. A symmetric cell was fabricated by sandwiching two identical electrodes around a 60-μm-thick hot-melt film (SX-1170-25, Solaronix). The cell was filled with a liquid electrolyte (0.6 M DMPII (1-propyl-2,3-dimethylimidazolium iodide), 0.1 M LiI, 0.05 M iodine, and 0.5 M TBP (4-tert-butylpyridine) in acetonitrile (AN)). The active electrode area of the cell was 0.283 cm^2. Impedance measurements were performed with a computer-controlled AUTOLAB/PGSTAT302N over a frequency range of 0.1–10^6 Hz with 5 mV ac amplitude.

2.4. DSSC assembly and photovoltaic performance

DSSCs employing the Pt-coated metallic substrates as the counterelectrodes were fabricated. A TiO_2 nanocrystalline photoanode (thickness: 15 ± 1 μm, Tripod Technology, Taiwan) was sintered at 450 °C for 30 min and then was immersed in an ethanol solution of N719 dye (0.4 mM) for 12 h. After dye adsorption, the photoanode was assembled with the counterelectrodes. The aforementioned hot-melt film was used as a spacer in between the two electrodes, and the liquid electrolyte was injected into the cell. Cell performance was evaluated under AM 1.5 (1 sun) illumination with a solar simulator (YSS-E40, Yamashita Denso Corp., Japan). Photocurrent–voltage (*J*–*V*) curves were recorded using a computer-controlled digital source meter (Keithley, model 2400). The active area of the cell was 0.283 cm^2.

3. Results and discussion

3.1. Analysis of the UV–vis spectrum of the plating solution

The UV–vis spectra of the H_2PtCl_6 plating solution were measured before and after reduction. Before reduction, the UV–vis spectrum of the solution exhibited an absorption peak at 260 nm due to the ligand-to-metal charge transfer transition of the $[PtCl_6]^{2-}$ ions [24]. After reduction, the absorption peak at 260 nm disappears, indicating that the $[PtCl_6]^{2-}$ ions have been completely reduced. Assuming that the reduced Pt atoms were completely deposited on the metallic substrates, the Pt loadings on the counterelectrodes were calculated to be 9.75, 19.5, 48.8, 97.5, 195, 487.5, and 975 μg/cm^2 at Pt concentrations of 3.12, 6.24, 15.6, 31.2, 62.4, 156, and 312 mg/L, respectively, as listed in Table 1.

Table 1
The calculated Pt loadings on the metallic substrates for various Pt concentrations of the plating solution.

Pt concentration of electroless solution (mg/L)	Calculated Pt loading ($\mu g/cm^2$)
312	975
156	487.5
62.4	195
31.2	97.5
15.6	48.8
6.24	19.5
3.12	9.75
Sputtered Pt	200[a]

[a] Data cited from Ref. [23] (Pt thickness = 100 nm).

3.2. Surface morphologies and roughness of chemically deposited and sputtered Pt layers on metallic substrates

Fig. 1 shows a series of SEM images that depict the surface morphologies of sputtered and chemically deposited Pt layers on Ni substrates. The sputtered Pt layer, as seen in Fig. 1(a), was quite flat and uniform. For the chemically deposited Pt layer, the surface morphologies varied with the Pt concentrations. At a Pt concentration of only 3.12 mg/L, many gray-white nanosized Pt particles (~10 nm in diameter) were distributed unevenly on the Ni substrate. As the Pt concentration increased, the Pt particles became larger and began to aggregate. When the Pt concentration reached 156 mg/L, the Pt particles increased to about 50–100 nm in diameter and connected with each other, but a continuous layer was not formed. At a Pt concentration of 312 mg/L, the morphology changed from granule to polyhedron, and the Ni substrate was completely covered by the polyhedron-shaped Pt particles. The AFM analysis revealed that the R_{rms} increases with increasing Pt concentration, as seen in Table 2, indicating that the surface roughness is improved by increasing the concentration of the Pt loading solution. The chemically deposited Pt layers exhibited R_{rms} values (4–58 nm) higher than the sputtered Pt layer (2.36 nm), which is in good agreement with the surface morphology shown in Fig. 1.

The surface morphologies of sputtered and chemically deposited Pt layers on stainless steel substrates are shown in Fig. 2. Similar to the Pt layers on Ni sheets described above, the sputtered Pt layers on stainless steel were also flat and uniform, as seen in Fig. 2(a). Very small Pt particles were distributed unevenly on the stainless steel when the chemically deposited Pt layer was prepared with a low concentration of Pt. When the Pt concentration was higher than 156 mg/L, the size of the granule-shaped Pt particles increased significantly, and the particles had diameters of approximately 50–100 nm. The Pt particles aggregated locally and began to

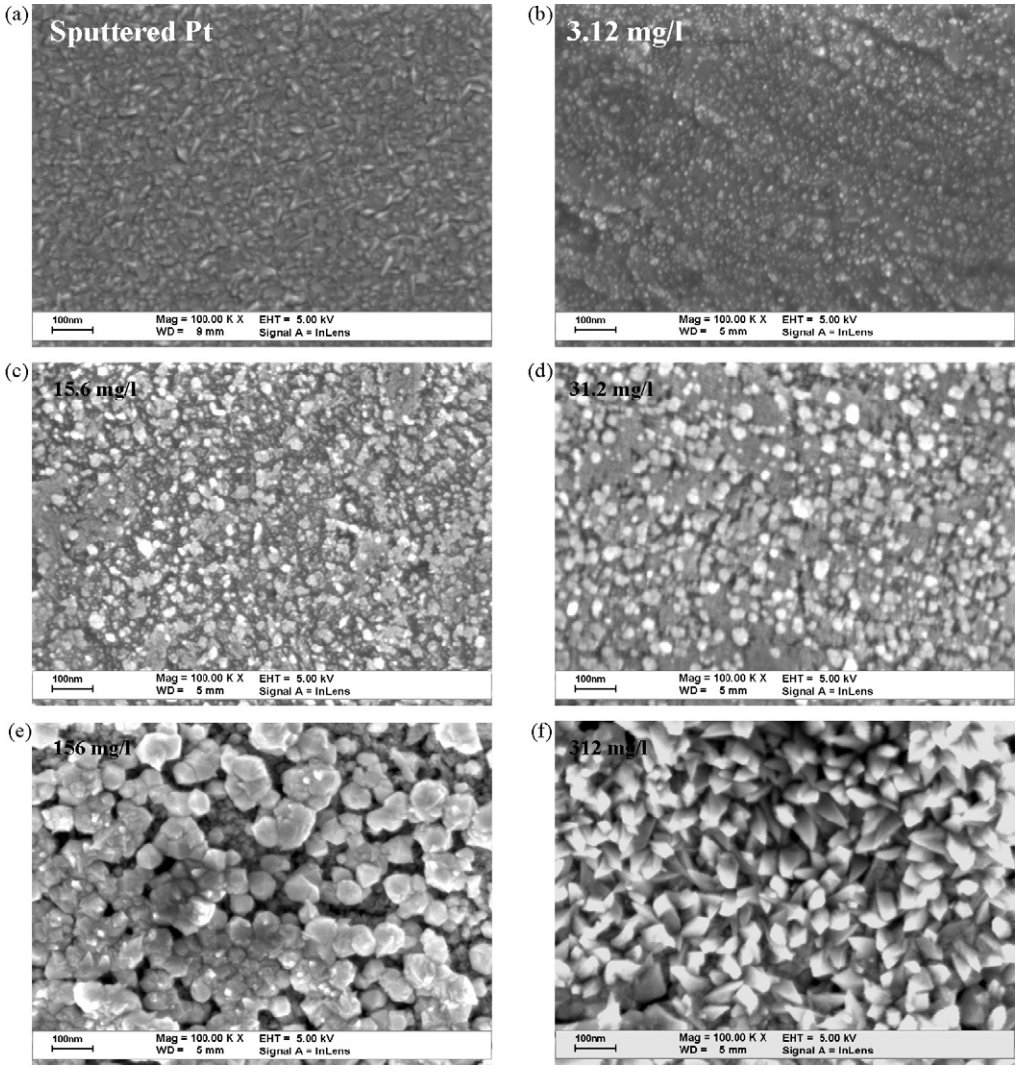

Fig. 1. The SEM micrographs showing the surface microstructures of (a) sputtered and (b–f) chemically deposited Pt layers on Ni substrates, where (b–f) were prepared with Pt concentrations of 3.12, 15.6, 31.2, 156, and 312 mg/L, respectively.

Table 2
The root-mean-square roughness (R_{rms}) of the Pt layers deposited on different metallic substrates with various Pt concentrations.

Counterelectrode		Pt concentration (mg/L)/Pt loading (μg/cm^2)	R_{rms} (nm)
Nickel	Electroless Pt	312/975	58.2
		156/487.5	34.7
		62.4/195	13.8
		31.2/97.5	8.8
		15.6/48.8	5.32
		6.24/19.5	5.12
		3.12/9.75	4.03
	Sputtered Pt	NA/200	2.36
Stainless steel	Electroless Pt	312/975	51.3
		156/487.5	28.8
		62.4/195	12.1
		31.2/97.5	7.23
		15.6/48.8	4.10
		6.24//19.5	2.16
		3.12/9.75	1.55
	Sputtered Pt	NA/200	1.36
Stainless steel (etched)	Electroless Pt	312/975	NA
		156/487.5	28.4
		62.4/195	28.7
		31.2/97.5	8.16
		15.6/48.8	5.19
		6.24/19.5	4.53
		3.12/9.75	4.08

stack vertically, as seen in Fig. 2(e) and (f). The chemically deposited Pt particles did not form a continuous layer on stainless steel, even at a Pt concentration of 312 mg/L. Some surface regions of the stainless steel substrate remained exposed, and this selective deposition of Pt reveals that the reactivity of the stainless steel towards chemical deposition was inconsistent. The Pt particles began to stack in the more reactive sites, and the regions that were left uncovered by the Pt particles were less reactive. Stainless steel consists mainly of iron, nickel, and chromium, and the selective chemical deposition of Pt may have been related to the variation of these components on the surface of the stainless steel. The surface roughness of the Pt layer also increased with increasing Pt concentrations, which is consistent with the R_{rms} results shown in Table 2.

To increase the surface area of stainless steel prior to the chemical deposition of Pt, an etching process was conducted by immersing the stainless steel in an acidic solution of 30 wt% H_2SO_4 at 60 °C for 5 min. The etched stainless steel exhibited a very rough and porous surface morphology (Fig. 3(a)), indicating that the etching process increased the surface area. After chemically depositing Pt (with a Pt concentration of less than 31.2 mg/L), the surface of stainless steel was still porous, as seen in Fig. 3(b). When the Pt concentration reached 156 mg/L, the deposited granule-shaped Pt nanoclusters almost covered the stainless steel and formed a nearly continuous layer. The porous appearance of the Pt layer was not evident, and the size of the Pt nanoclusters was smaller than that on un-etched stainless steel. The surface morphology of the

Table 3
The photovoltaic parameters obtained from the corresponding *J–V* curves shown in Fig. 4.

Counterelectrode		Pt concentration (mg/L)/Pt loading (μg/cm^2)	J_{SC} (mA/cm^2)	V_{OC} (V)	FF	η (%)
Nickel	Electroless Pt	312/975	15.34	0.69	0.67	7.08
		156/487.5	15.32	0.71	0.67	7.29
		62.4/195	15.15	0.69	0.66	6.89
		31.2/97.5	14.89	0.64	0.66	6.26
		15.6/48.8	14.72	0.66	0.64	6.18
		6.24/19.5	14.45	0.66	0.63	5.97
		3.12/9.75	14.28	0.67	0.58	5.54
	Sputtered Pt	NA/200	13.71	0.64	0.62	5.46
	Without Pt	NA/0	0.49	0.52	0.05	0.02
Stainless steel	Electroless Pt	312/975	15.08	0.67	0.62	6.18
		156/487.5	14.87	0.67	0.62	6.09
		62.4/195	14.74	0.66	0.64	6.35
		31.2/97.5	14.48	0.69	0.61	6.06
		15.6/48.8	14.34	0.64	0.63	5.80
		6.24/19.5	13.50	0.62	0.62	5.16
		3.12/9.75	10.69	0.65	0.61	4.24
	Sputtered Pt	NA/200	13.43	0.65	0.64	5.58
	Without Pt	NA/0	0.69	0.52	0.04	0.03
Stainless Steel (etched)	Electroless Pt	312/975		NA		
		156/487.5	15.17	0.68	0.65	6.68
		62.4/195	15.34	0.71	0.64	6.97
		31.2/97.5	14.33	0.68	0.66	6.35
		15.6/48.8	14.17	0.69	0.62	6.02
		6.24/19.5	13.89	0.66	0.63	5.74
		3.12/9.75	13.48	0.64	0.58	5.03

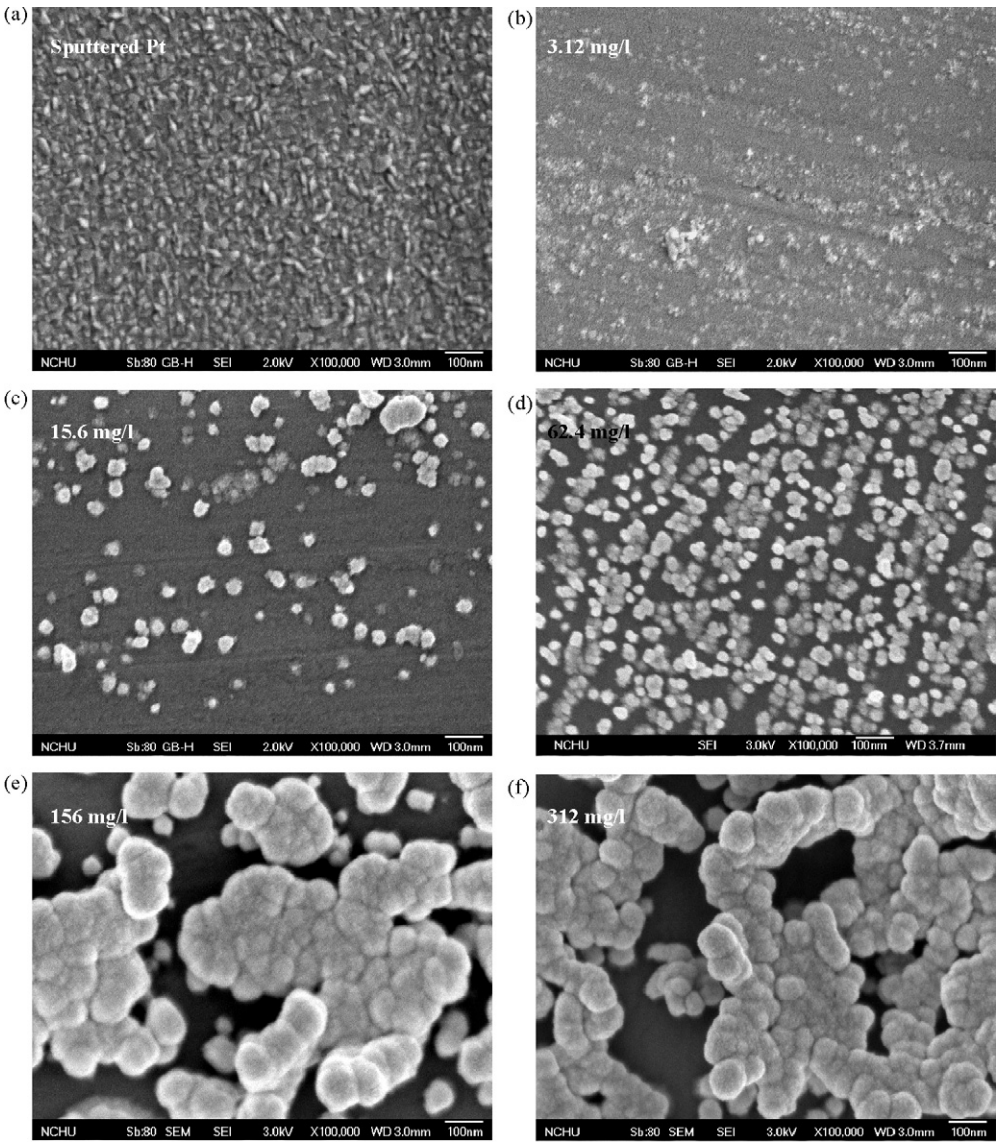

Fig. 2. The SEM micrographs showing the surface microstructures of (a) sputtered and (b–f) chemically deposited Pt layers on stainless steel substrates, where (b–f) were prepared with Pt concentrations of 3.12, 15.6, 62.4, 156, and 312 mg/L, respectively.

Pt layer prepared with the highest Pt concentration (312 mg/L) is not shown here because the resultant Pt layer easily detaches from the stainless steel, precluding subsequent analysis (e.g., AFM, EIS, and cell assembly). The corresponding R_{rms} values are similar to the previously mentioned two cases.

The above results demonstrate that the Pt layers deposited on un-etched and etched stainless steel show very different morphologies. Selective deposition of Pt was observed on un-etched stainless steel, while the Pt layer deposited on etched stainless steel showed better uniformity. As mentioned above, variation of the components of stainless steel is considered to be the cause of the selective deposition. To gain a better understanding of the correlation between selective Pt deposition and the components of the stainless steel, the surface compositions of un-etched and etched stainless steel substrates were analyzed using X-ray photoelectron spectroscopy (XPS). The XPS results indicate that the compositions of the un-etched and etched stainless steel substrates are 65 wt% Fe, 18.5 wt% Cr, 16.5 wt% Ni and 23.6 wt% Fe, 0.4 wt% Cr, 76 wt% Ni, respectively. The concentrations of iron and chromium decreased, but the concentration of nickel increased significantly after etching, indicating that the etching process primarily removes iron and chromium from the stainless steel, and the surface of the stainless steel becomes rich in nickel. Because the Pt layer deposited on etched stainless steel showed better uniformity than that on un-etched stainless steel (Fig. 2 versus Fig. 3), it is reasonable to infer that nickel has higher activity for the chemical deposition of Pt. In other words, because the un-etched stainless steel had a lower nickel concentration (16.5 wt%), its activity towards the chemical deposition of Pt was lower, and thus the deposition took place selectively in the nickel-rich areas. The etched stainless steel had a higher nickel composition (76 wt%), which significantly increased its activity towards the chemical deposition of Pt. Therefore, the deposited Pt layer showed better uniformity.

Inspection of Table 2 reveals that the chemically deposited Pt layer on a Ni substrate exhibited the highest surface roughness compared with the other two substrates. In addition, the surface roughness of the Pt layer deposited on etched stainless steel was higher than that on the stainless steel without etching pre-treatment (with a Pt concentration of less than 62.4 mg/L). This higher surface roughness is due to the fact that the Pt layer deposited on the etched stainless steel exhibited a porous structure (Fig. 3), which can make the surface rougher. However, the

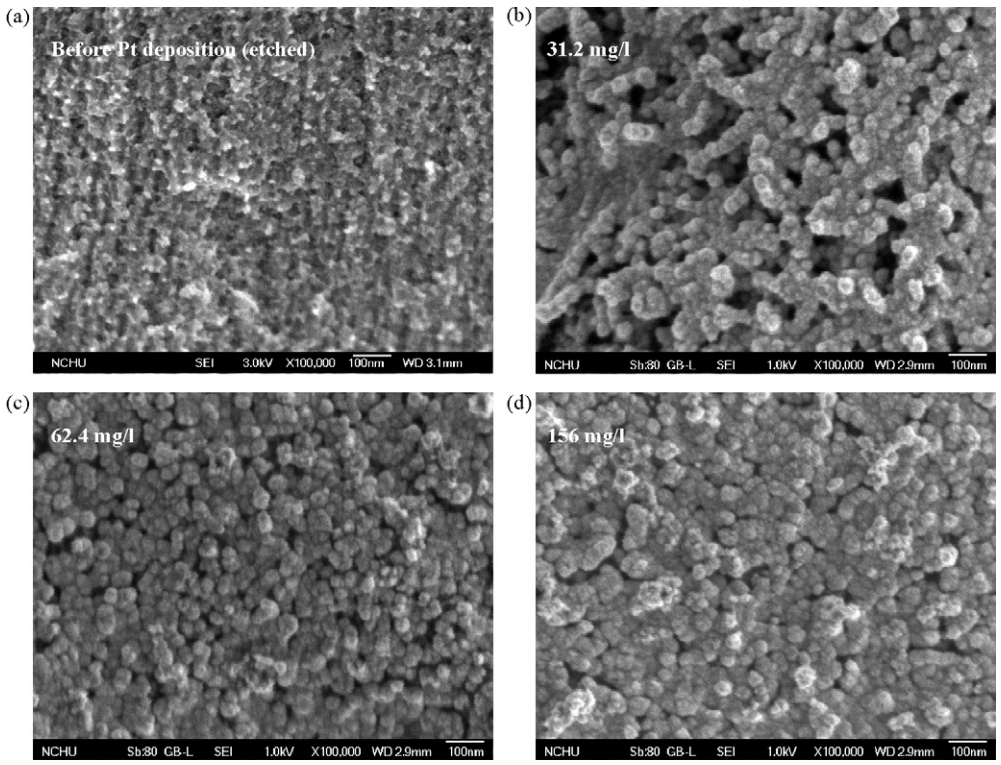

Fig. 3. The SEM micrographs showing the surface microstructures of (a) as-etched stainless steel and (b–d) chemically deposited Pt layers on etched stainless steel substrates, where (b–d) were prepared with Pt concentrations of 31.2, 62.4, and 156 mg/L, respectively.

R_{rms} values of the Pt layer deposited on etched stainless steel decreased slightly as the Pt concentration was increased from 62.4 to 156 mg/L. As mentioned above, a continuous Pt layer without evident pores was formed on the etched stainless steel when the Pt concentration is 156 mg/L (Fig. 3(d)). This continuous layered structure is likely the cause of the decrease in the R_{rms} value. At this Pt concentration (156 mg/L), the R_{rms} value of the Pt layer on etched stainless steel was smaller than that on the un-etched stainless steel. This result can be explained by comparing Figs. 2(e) and 3(d); the Pt nanoclusters deposited on un-etched stainless steel exhibited a rougher surface structure, but the Pt particles on etched steel formed a uniform and continuous layer.

3.3. Photovoltaic performance of DSSCs based on Pt-coated metallic counterelectrodes

The *J–V* curves of the as-fabricated DSSCs are shown in Fig. 4, and the corresponding photovoltaic parameters are listed in Table 3. For DSSCs employing bare metallic substrates (without a Pt coating) as counterelectrodes, the energy conversion efficiencies (η) were only

Table 4
The electrochemical impedance spectroscopy (EIS) data deduced from Fig. 6.

Counterelectrode		Pt concentration (mg/L)/Pt loading (μg/cm^2)	R_S (Ω cm^2)	R_{CT} (Ω cm^2)	CPE: β	CPE: B
Nickel	Electroless Pt	312/975	0.302	0.66	0.92	1.58×10^{-4}
		156/487.5	0.377	1.72	0.89	3.24×10^{-4}
		62.4/195	0.308	2.09	0.87	2.19×10^{-4}
		31.2/97.5	0.312	2.87	0.88	1.15×10^{-4}
		15.6/48.8	0.317	3.62	0.88	1.22×10^{-4}
		6.24/19.5	0.301	4.37	0.91	3.61×10^{-5}
		3.12/9.75	0.299	4.95	0.91	3.2×10^{-5}
	Sputtered Pt	NA/200	0.56	3.18	0.93	5.7×10^{-5}
Stainless steel	Electroless Pt	312/975	0.521	2.21	0.87	1.38×10^{-4}
		156/487.5	0.549	3.58	0.89	7.07×10^{-5}
		62.4/195	0.544	4.18	0.91	3.03×10^{-5}
		31.2/97.5	0.554	5.03	0.90	7.3×10^{-5}
		15.6/48.8	0.543	5.53	0.91	7.96×10^{-5}
		6.24/19.5	0.502	10.4	0.90	4.47×10^{-5}
		3.12/9.75	0.584	36.1	0.90	1.96×10^{-5}
	Sputtered Pt	NA/200	0.64	3.2	0.94	5.42×10^{-5}
Stainless steel (etched)	Electroless Pt	312/975			NA	
		156/487.5	0.706	1.23	0.87	3.24×10^{-4}
		62.4/195	0.769	2.47	0.87	8.21×10^{-4}
		31.2/97.5	0.721	4.21	0.87	1.1×10^{-4}
		15.6/48.8	0.697	7.65	0.89	8.02×10^{-5}
		6.24/19.5	0.782	8.25	0.90	1.94×10^{-5}
		3.12/9.75	0.743	10.3	0.90	1.93×10^{-5}

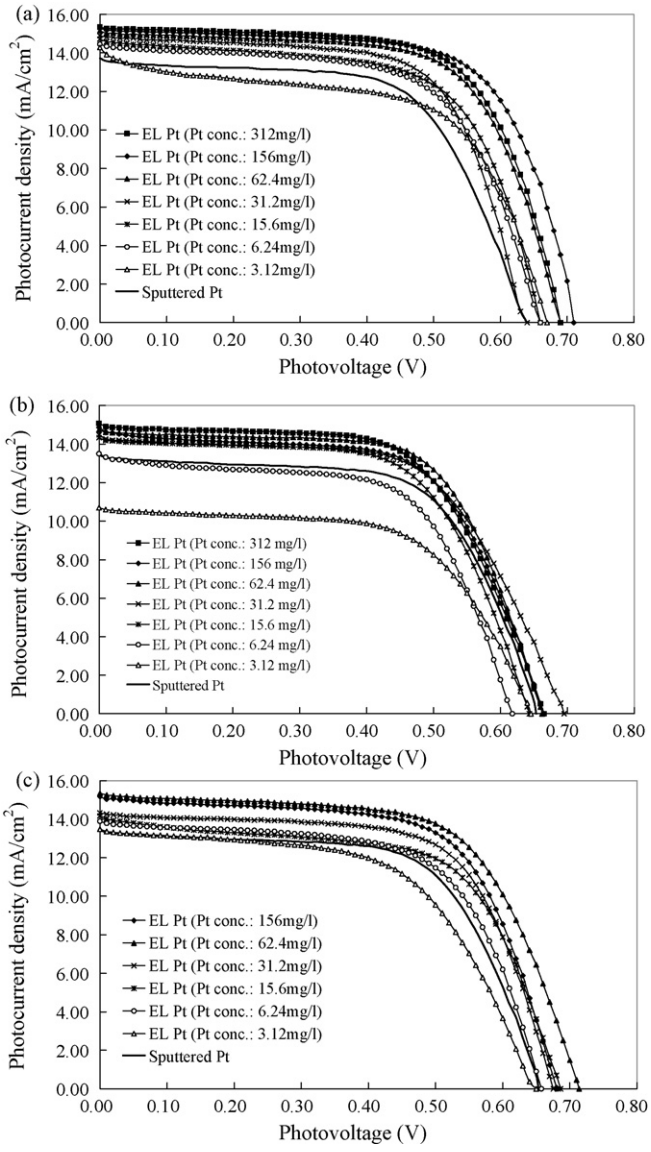

Fig. 4. The *J–V* curves of the DSSCs employing three types of metallic substrates coated with chemically deposited or sputtered Pt layers as the counterelectrodes. The metallic substrates are (a) Ni, (b) stainless steel, and (c) etched stainless steel.

0.02–0.03%. However, η increased dramatically when a Pt layer was deposited on the metallic substrates, indicating that the catalytic Pt is necessary to obtain well-configured DSSCs. A comparison of the photovoltaic parameters reveals that the increase in η can be attributed to an increase in both the short-circuit current density (J_{SC}) and the fill factor (FF), while the contribution from the open-circuit voltage (V_{OC}) is less significant. By utilizing the excellent catalytic performance of Pt, the charge transfer is less resistive at the electrolyte/Pt interface compared to the electrolyte/Ni (or stainless steel) interface, and therefore the J_{SC} increases. Because the FF depends strongly upon the internal resistance of the cell, a higher FF can be obtained for the cells with a Pt-coated counterelectrode due to a lower resistance of charge transfer at the electrolyte/Pt interface.

For the DSSC that employed a Ni sheet coated with a sputtered Pt layer as the counterelectrode, the η value was 5.46%. The η value increased when the catalytic Pt layer was prepared by chemical deposition with a Pt concentration higher than 3.12 mg/L. The η value of the cell increased by 26% when the Pt concentration was 62.4 mg/L and when the corresponding Pt loading was 195 μg/cm^2 (similar to that of the sputtered Pt layer (200 μg/cm^2)). The improved efficiency is mainly attributed to the increase of J_{SC} from 13.71 to 15.15 mA/cm^2. The η value of the DSSC based on chemically deposited Pt increased as the Pt concentration of the plating solution increased. The improved efficiency is also a result of the increase in both J_{SC} and FF. The η value exceeds 7% when the Pt concentration is increased to 156 mg/L.

The direct correlation between J_{SC} and the amount of Pt loading is due to the increasing surface area of the Pt layer as the concentration of the Pt loading solution was increased. As shown in Fig. 1, the Pt layer prepared by chemical deposition exhibited a porous structure when the Pt loading concentration increases, indicating that the surface became rougher with increasing concentrations of the Pt loading solution. R_{rms} measurements (Table 2) show similar results. The increase in surface roughness implies that the surface area for catalytic reaction increased. In other words, the charge transfer resistance (R_{CT}) at the electrolyte/Pt interface can be reduced by increasing the Pt loading (the R_{CT} will be discussed in the next section). Because electrons can be transferred at a faster rate in the I^-/I_3^- reduction, the J_{SC} increases with increasing concentrations of the Pt loading solution. This phenomenon has been observed previously [18,20,22,25], but was not obvious when the Pt layer is prepared by sputtering. The sputtered Pt layer had a dense structure and presented a very uniform surface morphology across a broad range of the Pt loadings (thickness) [13]. The surface area and R_{CT} will not change markedly with the increase of the Pt loading, and therefore, the change in J_{SC} was insignificant.

For the DSSC that employed a stainless steel coated with a sputtered Pt layer as the counterelectrode, the η value was 5.58%, which is very close to that based on a Ni sheet. Similarly, the η value of the DSSC increased with increasing Pt concentrations when the catalytic Pt layer was prepared by chemical deposition. Obviously, higher η values were obtained as a result of higher J_{SC} values. The DSSCs based on stainless steel exhibited efficiencies lower than those employing Ni sheets. Once again, J_{SC} and FF were found to be the major factors that determine the cell efficiency. It is interesting to find that the η value can be increased by 4–19% when an etched stainless steel was employed as the substrate for the counterelectrode. The DSSC based on an etched stainless steel also possessed better photovoltaic performance (J_{SC}, V_{OC}, and FF) than that based on an un-etched stainless steel.

3.4. EIS analysis of the Pt-coated counterelectrodes and the correlation with the photovoltaic performance of the DSSC

To further study the electrochemical characteristics of platinized metallic substrates, the EIS analysis was performed on a symmetric cell fabricated by two identical platinized electrodes. According to the EIS theory, the ideal Nyquist plot of the cell includes a series resistance (R_S) in the high-frequency region, an R_{CT} in the medium-frequency region, and a Nernst diffusion impedance (R_D) in the low-frequency region [25], as shown in Fig. 5. C_{DL} refers to the double-layer capacity. The intercept of the real axis refers to the R_S, which includes the sheet resistances of the two identical platinized electrodes and the electrolytic resistance [10]. Because the electrolytic resistance is usually very low for liquid-type electrolytes, the contribution to the measured R_S mainly comes from the sheet resistance of platinized electrodes [15]. The diameter of the left-hand semicircle represents the R_{CT} of the triiodide reduction at the electrolyte/Pt interface [14]. Owing to the symmetric configuration of the cell, the real R_{CT} value should be half of the diameter. In general, the catalytic performance of the platinized electrode can be estimated qualitatively from the R_{CT} value.

Fig. 6 shows the real Nyquist plots of the symmetric cells fabricated with the aforementioned three types of platinized metallic

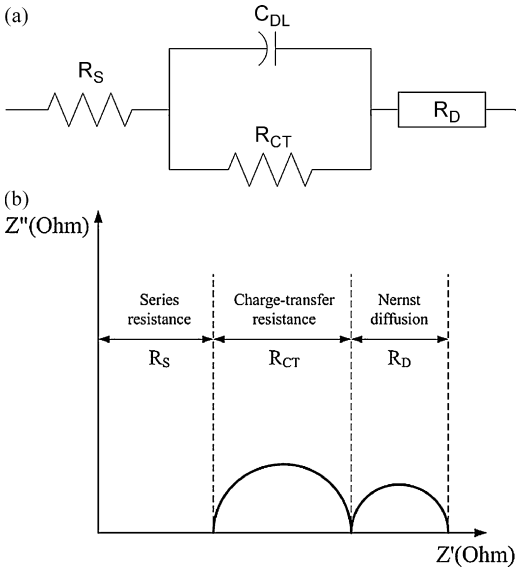

Fig. 5. (a) The circuit of a symmetric cell fabricated by two identical platinized electrodes. (b) The corresponding ideal Nyquist plot of the symmetric cell.

substrates. Based on Fig. 6, the R_S and R_{CT} values for chemically deposited and sputtered Pt electrodes can be deduced and are listed in Table 4. For the three types of metallic substrates coated with Pt via chemical deposition, the cell employing a Ni sheet as the electrode exhibited the lowest R_S, while that employing an etched stainless steel surface showed the highest R_S. Because Ni inherently possesses a sheet resistance ($3.5 \times 10^{-4}\ \Omega/\square$) lower than that of stainless steel ($3.8 \times 10^{-3}\ \Omega/\square$) [22], the cell based on the Ni substrate was expected to have a lower R_S. For the etched stainless steel, the porous surface structure slows the electron motion, and therefore, the cell based on this type of metallic substrate showed the highest R_S.

The cell based on the Ni substrate also exhibited the lowest R_{CT}, implying that the catalytic activity is best when the Pt layer is deposited on a Ni substrate using chemical deposition. As mentioned previously (Table 2), the Pt layer deposited on a Ni substrate using chemical deposition shows the highest surface roughness (R_{rms}). Therefore, the larger surface area improves charge transfer as well as triiodide reduction, and the lowest R_{CT} is obtained. With the lowest R_S and R_{CT}, a better FF can be obtained due to the reduced internal resistance. Similarly, a higher J_{SC} can also be achieved, and the DSSC employing a Ni substrate coated with Pt by chemical deposition as the counterelectrode shows the best η value of the three types of DSSCs (Table 3).

Inspection of Table 4 reveals that the three types of cells show similar trends in the R_{CT} dependence, i.e., the R_{CT} decreased with increasing the Pt concentration. The reduction of R_{CT} indicates that the charge transfer became more effective at the electrolyte/Pt interface, which is a result of the increased surface area of the chemically deposited Pt layer when higher Pt concentrations were used. The microstructures of the chemically deposited Pt layer (shown in Figs. 1–3) and the R_{rms} variations (listed in Table 2) show that the surface roughness of chemically deposited Pt layer increases with increasing the Pt concentration. To further examine the correlation of the Pt concentration with the active surface area of chemically deposited Pt for catalytic reactions, the constant phase element (CPE) was examined. The impedance Z_{CPE} of a CPE can be expressed as [26]

$$Z_{CPE} = B(j\omega)^{-\beta} \quad (1)$$

where B is the CPE parameter, ω is the angular frequency, and β is the CPE component, which ranges from 0 to 1. When β equals to

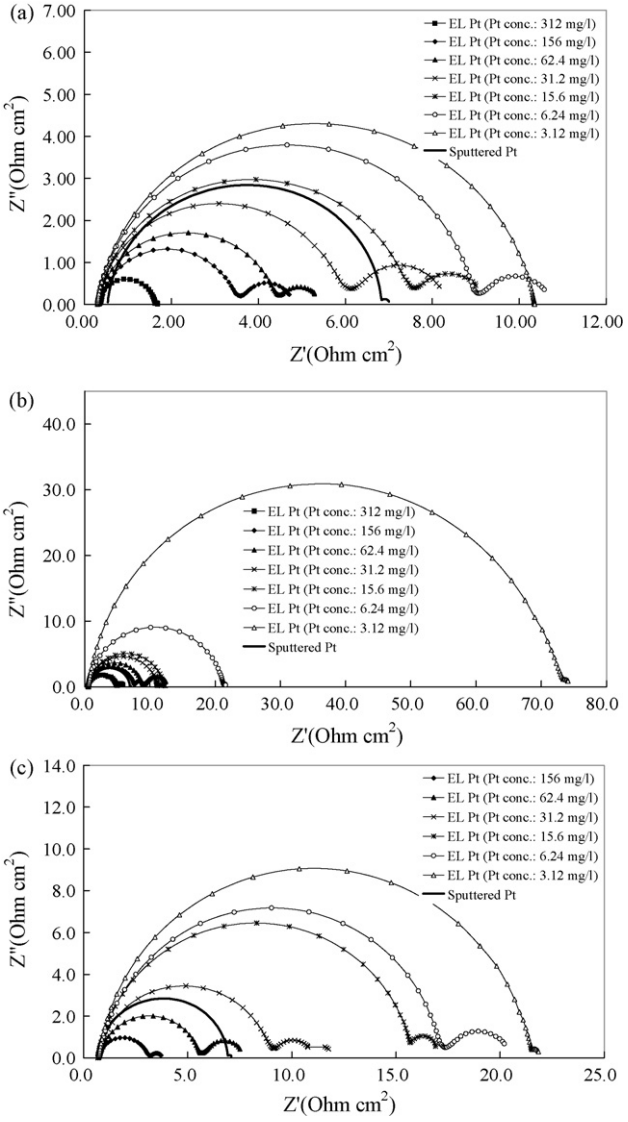

Fig. 6. Real Nyquist plots of the symmetric cells based on three types of metallic substrates coated with chemically deposited or sputtered Pt. The metallic substrates are (a) Ni, (b) stainless steel, and (c) etched stainless steel.

1, the CPE will represent a perfect capacitor and the corresponding impedance spectrum will exhibit an ideal semicircle. However, the impedance spectrum of the electrolyte/Pt interface usually deviates slightly from the ideal semicircle due to the roughness and porosity of the Pt surface, making β less than 1. The β values are listed in Table 4. It was found that β generally decreases with increasing the Pt concentration, indicating that increasing the Pt concentration can improve the roughness/porosity of the electrode surface. This tendency is in agreement with the aforementioned microstructure changes and with the R_{rms} variation of chemically deposited Pt layers. Consequently, the chemically deposited Pt layers prepared with high Pt concentrations offer a larger surface area for catalytic reactions. The J_{SC} and FF both increase with increasing Pt concentrations and thereby improve the cell efficiency, as shown in Table 3.

As mentioned above (Table 3), the DSSC employing an etched stainless steel substrate in the counterelectrode exhibits better efficiency than that based on un-etched stainless steel. From Table 2, it is clear that this increase in efficiency is primarily due to the higher surface roughness (R_{rms}) of the Pt layer deposited on etched stainless steel; this rougher surface offers a larger surface area for triiodide reduction and thereby increases the J_{SC}. The β val-

ues listed in Table 4 also show the same results, i.e., that the β value of the Pt layer deposited on etched stainless steel is smaller than that for un-etched stainless steel, indicating that the Pt layer deposited on etched stainless steel has a rougher surface morphology. Because the Pt layer with a rougher surface morphology can offer a larger surface area for catalytic reaction, the charge transfer on the rougher Pt surface will be less resistive, and therefore, a lower R_{CT} can be obtained, which is also an influential factor for improving the efficiency of DSSCs.

An R_{CT} value of less than $10\,\Omega\,cm^2$ is essential for a Pt-coated counterelectrode to have an acceptable catalytic capability [12]. Based on the data listed in Table 4, the majority of the R_{CT} values are lower than $10\,\Omega\,cm^2$, indicating that chemical deposition is a promising method for growing catalytic Pt layers on metallic substrates for use as counterelectrodes in DSSCs.

4. Conclusions

Chemical deposition was successfully employed to grow catalytic Pt layers on nickel sheets and stainless steel, and the resulting Pt-coated metallic sheets were used as the counterelectrodes in DSSCs. The chemically deposited Pt layers exhibited higher surface roughness as the Pt concentration of the plating solution increased. Therefore, a larger Pt surface area can be provided for charge transfer, reducing the charge transfer resistance at the electrolyte/Pt interface and promoting the triiodide reduction reaction. The short-circuit current is then raised. As a result, the cell efficiency increases with increasing Pt concentrations of the plating solution. The DSSC employing a Ni sheet coated with chemically deposited Pt as the counterelectrode exhibited better photovoltaic performance compared with on the use of a stainless steel counterelectrode. This result is attributed to the fact that the Pt-coated Ni counterelectrode simultaneously has lower series and charge transfer resistances. The lower series resistance is due to the inherently lower sheet resistance of Ni, and the lower charge transfer resistances are caused by the very rough and porous structure of the chemically deposited Pt layer on the Ni sheet. This rough surface can provide a larger electrolyte/Pt interfacial area for charge transfer. Both effects can reduce the energy lost in electron transfer and can improve the photovoltaic performance. The conversion efficiencies of DSSCs based on Pt-coated metallic counterelectrodes range from 4% to 7%, and the best efficiency (7.29%) was obtained with the DSSC that employed a Ni sheet coated with chemically deposited Pt as the counterelectrode.

Acknowledgements

The authors wish to acknowledge financial support from the National Science Council of Taiwan, ROC through Grant NSC 96-ET-7-005-001-ET. This work was supported in part by the Ministry of Education, Taiwan, ROC under the ATU plan.

References

[1] M. Grätzel, Nature 414 (2001) 338.
[2] B. O'Regan, M. Grätzel, Nature 353 (1991) 737.
[3] L.M. Peter, K.G.U. Wijayantha, Electrochim. Acta 45 (2000) 4543.
[4] A. Kay, M. Grätzel, Sol. Energy Mater. Sol. Cells 44 (1996) 99.
[5] K. Suzuki, M. Yamaguchi, M. Kumagai, S. Yanagida, Chem. Lett. 32 (2003) 28.
[6] T.N. Murakami, S. Ito, Q. Wang, M.K. Nazeeruddin, T. Bessho, I. Cesar, P. Liska, R. Humphry-Baker, P. Comte, P. Páchy, M. Grätzel, J. Electrochem. Soc. 153 (2006) A2255.
[7] K. Imoto, K. Takatashi, T. Yamaguchi, T. Komura, J. Nakamura, K. Murata, Sol. Energy Mater. Sol. Cells 79 (2003) 459.
[8] T. Hino, Y. Ogawa, N. Kuramoto, Carbon 44 (2006) 880.
[9] Y. Saito, T. Kitamura, Y. Wada, S. Yanagida, Chem. Lett. 31 (2002) 1060.
[10] Y. Saito, W. Kubo, T. Kitamura, Y. Wada, S. Yanagida, J. Photochem. Photobiol. A: Chem. 164 (2004) 153.
[11] K.M. Lee, P.Y. Chen, C.Y. Hsu, J.H. Huang, W.H. Ho, H.C. Chen, K.C. Ho, J. Power Sources 188 (2009) 313.
[12] A. Hauch, A. Georg, Electrochim. Acta 46 (2001) 3457.
[13] X. Fang, T. Ma, G. Guan, M. Akiyama, T. Kida, E. Abe, J. Electroanal. Chem. 570 (2004) 257.
[14] N. Papageorgiou, W.F. Maier, M. Grätzel, J. Electrochem. Soc. 144 (1997) 876.
[15] G. Wang, R. Lin, Y. Lin, X. Li, X. Zhou, X. Xiao, Electrochim. Acta 50 (2005) 5546.
[16] S. Hao, J. Wu, J. Lin, Y. Huang, Compos. Interfaces 13 (2006) 899.
[17] N. Papageorgiou, Coord. Chem. Rev. 248 (2004) 1421.
[18] S. Kim, Y. Nah, Y. Noh, J. Jo, D. Kim, Electrochim. Acta 51 (2006) 3814.
[19] P. Li, J. Wu, J. Lin, M. Huang, Z. Lan, Q. Li, Electrochim. Acta 53 (2008) 4161.
[20] C.H. Yoon, R. Vittal, J. Lee, W.S. Chae, K.J. Kim, Electrochim. Acta 53 (2008) 2890.
[21] Y. Chiba, A. Islam, Y. Watanabe, R. Komiya, N. Koide, L. Han, Jpn. J. Appl. Phys. 45 (2006) L638.
[22] T. Ma, X. Fang, M. Akiyama, K. Inoue, H. Noma, E. Abe, J. Electroanal. Chem. 574 (2004) 77.
[23] T.C. Wei, C.C. Wan, Y.Y. Wang, Appl. Phys. Lett. 88 (2006) 103122.
[24] T. Teranishi, M. Hosoe, T. Tanaka, M. Miyake, J. Phys. Chem. B 103 (1999) 3818.
[25] T.C. Wei, C.C. Wan, Y.Y. Wang, C.M. Chen, H.S. Shiu, J. Phys. Chem. C 111 (2007) 4847.
[26] J.R. Macdonald, Impedance Spectroscopy, Wiley, New York, 1987.